Regenerated Bamboo-Derived Cellulose Fibers/RGO-Based Composite for High-Performance Supercapacitor Electrodes

Tianhao Wang,[1] Wentao Zhang,[1] Shujuan Yang,[1] Weiqian Tian[2] and Liping Zhang[*1]

1 Department of Material Science and Technology, MOE Key Laboratory of Wooden Material Science and Application, Beijing Forestry University. No.35, Tsinghua East Road, Haidian District, Beijing, China.
2 Department of Fibre and Polymer Technology, KTH Royal Institute of Technology, Teknikringen 56, 10044 Stockholm, Sweden
E-mail address: Zhanglp418@163.com (L.P. Zhang)

Abstract. Bamboo-derived cellulose fibers/RGO carbon aerogel composite was prepared by using a facile aerogel-based method, in which bamboo pulp fibers were dissolved and incorporated in an ionic liquid system, and RGO was introduced by thermal reduction approach. The obtained bamboo-derived cellulose fibers/RGO carbon aerogel composite shows a large specific surface area, and excellent electrochemical performance. When the GO content was 2.5 wt%, the obtained composite showed a high specific surface area of 1957 m^2/g, and high specific capacitance of 351 F/g in 6 M KOH electrolyte solution even with a more than 90% capacitance retention at a high scan rate of 200 mV/s. The bamboo-derived cellulose fibers/RGO composite electrodes show the low equivalent series resistance of 5.0 Ω and small charge transfer resistance of 0.30 Ω which further demonstrate the excellent electrochemical behaviors.

1. Introduction

Shortages of fossil fuels and climate change are serious problems associated with environmental pollution; hence, there is an urgent need for highly efficient and low-cost sustainable energy storage devices. Among energy storage systems, electrochemical capacitors (supercapacitors) have good cycle stability, high power densities, and environment-friendly [1]. In recent years, supercapacitors have drawn interest in the applications for hybrid vehicles and portable electronic devices [2]. While increasing the specific surface area of the electrode material, increasing the conductivity of the material can effectively improve the performance of the supercapacitor [3]. Carbon nanomaterials can well meet these requirements. Among carbon nanomaterials, graphene has the characteristics of good electrical conductivity, high specific surface area, high heat resistance and good chemical stability. It is the most commonly used electrode material of supercapacitor at present [4].

However, due to the high preparation cost, easy agglomeration and low reaction capacity of graphene. Therefore, reduced graphene oxide (RGO) is often used as an additive to the electrode material of supercapacitors, and graphene alone is rarely used as the electrode material [5]. After a simple carbonization process, the biomass porous carbon material can have a high specific surface area, which is very helpful to improve the specific surface area of the supercapacitor electrode. Meanwhile, in this process, the pore diameter and pore distribution of biomass porous carbon materials can be adjusted by the conditions of carbonization process. In this way, the optimal pore structure and specific surface area can be obtained, which is conducive to improving the capacity of

supercapacitors to store electrical energy [6]. Among the numerous biomass porous carbon materials, bamboo has the advantages of wide distribution, fast growth cycle and high economic effect. Therefore, we prepared the supercapacitor electrode with bamboo cellulose fibers as the main material.

Then, in order to improve the specific surface area of the composites, we prepared porous carbon composites by using the strategy based on carbon aerogel and high temperature activation method. Carbon aerogel has large specific surface area, good chemical stability and high porosity. Low density, three-dimensional network structure. These characteristics enable electrolytes to enter mpterial interior for energy storage [7].

To sum up, the experiment we here dissolved bamboo cellulose in a quaternary ammonium salt ionic liquid, which disrupted the structure of the cellulose to release the internal hydrogen-bonded molecular chains. We used this solution to produce carbon aerogels with a porous structure to realize the high specific surface area of composite materials, and added oxidized graphene to improve the conductivity of the composite materials. We examined the effects of different mass loading of RGO onto the performance as a supercapacitor electrode material in 6 M KOH aqueous electrolyte.

2. Experimental

2.1. Materials

Bamboo pulp (constituents listed in Table 1), was provided by Jilin Chemical Fibers Co., Ltd., Jilin, China. Tetrabutylammonium acetate (IL) was purchased from Tokyo Chemical Industry Co., Ltd., Shanghai, China. Graphene oxide was provided by Jining Lite Nanotechnology Co., Ltd., Shandong, China. Dimethyl sulfoxide (DMSO), polyvinylidene fluoride, N-methyl pyrrolidone, and hydrochloric acid were purchased from Beijing Chemical Works, Beijing, China. Potassium hydroxide was purchased from Xilong Chemical Co., Ltd., Hubei, China. Deionized water was used throughout the experiments.

Table 1. Compositions of Bamboo Pulp Fibers

Sample	Degree of polymerization	α-Cellulose (wt%)	Moisture (wt%)	Cellulose (wt%)	Hemicellulose (wt%)	Lignin (wt%)
Pulp Fibers	728	82.6	5.6	92.8	2.3	4.5

2.2. Preparation of Cllulose Fbers/GO Arogel

A cellulose solvent was prepared by mixing the tetrabutylammonium acetate with the cosolvent of DMSO, and then different proportions of GO (i.e., 1.5 wt%, 2.5 wt%, and 3.5 wt%) were added into it. 5 wt% bamboo pulp fibers were dissolved in the cellulose solvent at room temperature over 48 h. After that, A regenerated cellulose alcohol gel was obtained by solvent exchange with deionized water and tert-butanol. The gel was frozen in liquid nitrogen for 5 min before freeze-drying (-60℃, 40 Pa) for 48 h. Finally regenerated cellulose/GO aerogel obtained, was denoted as RA_x, where x refers to the content of GO.

2.3. Carbonization and Ativation

The regenerated cellulose/GO aerogels were carbonized in a tuber furnace under N_2 atmosphere from room temperature at a rate of 5 ℃/min up to 900 ℃ for 1 h. The samples were then cooled to room temperature, and cellulose/GO-derived carbon aerogels were obtained as CRA_x, where x refers to the different proportion of GO. In the subsequent activation process, we used KOH as an activator with a 1:2 ratio of carbon aerogel and KOH.

In brief, the carbon aerogels were immersed in KOH solution and then were heat at 100 ℃ in an oven to evaporate the excess water. The resulting mixture was transferred to a tuber furnace and heated in N_2 atmosphere from room temperature to 900 ℃ at a rate of 5 ℃/min and maintained at that temperature for 1 h before cooling to room temperature. We used 1 M HCl and deionized water to wash the sample until the pH up to neutral. We used the bamboo-derived cellulose fibers/RGO carbon

aerogel composite, denoted as A-CRA$_x$, where x represents the different proportions of GO added.

2.4. Characterization

The morphology of the prepared sample was investigated with a scanning electron microscope (SEM, S-3000n, Hitachi, Japan). X-ray diffractometer (XRD) patterns were obtained from a powder X-ray diffractometer (Bruker D8 Advance) with Cu-Ka radiation at 40 kV and 40 mA. XRD data were collected in continuous scan mode from 10° to 50°, with a step size of 0.01°. FT-IR spectra were acquired on a Bruker Vector 33 spectrometer with KBr pellets. The reflectance spectra were measured over the energy range of 400 to 4000 cm^{-1} at a spectral resolution of 4 cm^{-1} with 32 scans. Thermogravimetric analysis (TGA) was studied in a TGA-600 analyzer (Shimadzu, Japan). Samples (5-10 mg) were heated up to 600 ℃ at a rate of 20 ℃/min, and the flow rate of nitrogen was 20 mL/min. The porous features were determined by using a Micromeritics analyzer (ASAP 2460) at 77 K, with the degassing time of 10 h and the degassing temperature at 200 ℃. The specific surface area was calculated by the Brunauer-Emmett-Teller method (BET) method based on adsorption data in the relative pressure (P/P0) range from 0.06 to 0.20 and total pore volume was obtained at a relative pressure (P/P0) of 0.99 from the amount of adsorbed nitrogen. The pore size distributions (PSDs) were calculated by using non-local density functional theory (NLDFT) method.

2.5. Electrochemical Aalysis

We used a three-electrode system to characterize the electrochemical properties of the sample. In three-electrode system, Pt metal and saturated Ag/AgCl calomel electrodes were used as the counter and reference electrodes, respectively. The electrolyte used was 6 M KOH solution. The work electrode was prepared as follows: the sample was ground in an agate mortar, and was then mixed with PVDF, acetylene black in NMP to obtain slurry which was pressed onto the nickel foam as thin slices and dried in an oven.

The electrochemical performances of the materials were evaluated with a CHI 760D electrochemical station (CH Instruments, USA) by Cyclic voltammetry (CV), galvanostatic charge/discharge (GCD) measurements, and electrochemical impedance spectrogram (EIS) techniques. CV curves were measured at different potential sweep rates of 10-200 mV/s within the potential window of 0-0.9 V. The gravimetric specific capacitances were calculated from the CV curves according to the equation $C = \int IdV/(\upsilon m\Delta V)$, where I is the current (A), ΔV is the working voltage window (V), m is the mass of active material (g), and v is the scan rate (mV/s). GCD w performed at a different current densities in the range of 0.5-10 A/g (with a potential window of 0-0.9 V). The specific capacitances were calculated from the discharge curves by the equation of $C = I\Delta t/(m\Delta V)$, where I is the discharge current (A), Δt is the discharge time(s), ΔV is the working voltage window (V). Finally, EIS was conducted in the frequency range from 0.01 Hz to 100 kHz.

3. Results and Discussion

3.1. Synthesis of Prous A-CFA

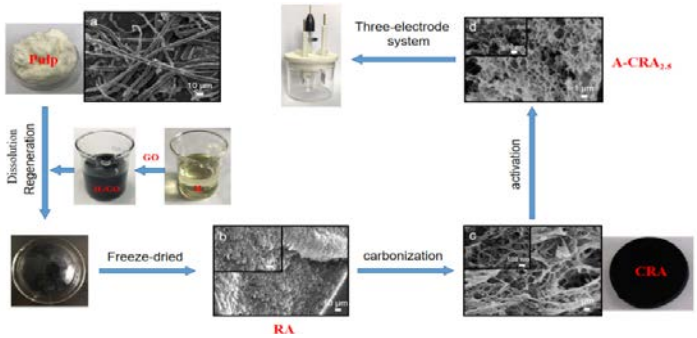

Figure 1. Schematic Ilustration of the Fbrication Pocess of A-CFA: FE-SEM of Pristine Bamboo Pulp Fibers (a), RA (b), CRA (c) and A-CRA$_{2.5}$ (d)

Figure 1 shows the schematic of the fabrication of A-CFA and the SEM images of A-CRA and A-CRA$_{2.5}$. The bamboo pulp fibers showed a rod-like structure with a diameter of approximately 6-8 μm (Figure 1a). After the bamboo pulp fibers were added to the tetrabutylammonium acetate/DMSO ionic liquid system, they swelled and intra- and inter-molecular hydrogen bonding was partially disrupted. In the process of regeneration, the broken cellulose molecular chains became unstable and rearranged to a stable crystalline structure.

SEM images show that many micropores were generated on the surface of the bamboo fibers surface after the activation treatment. Similar to other biomass-derived carbon products obtained by KOH activation [8], A-CRA$_{2.5}$ had disordered and wormlike micropores, other than that we can see RGO was implanted in the structure of A-CRA. Thus, the chemical activation effectively increased the porosity of the walls of the fiber. The surface of the bamboo pulp fibers was uneven, and microfibers aggregates were visible. In the regenerated aerogel (Figure 1b), a large number of pore structures appeared on the surface of the aerogel, and large voids appeared in the structure.

These features provided a large specific surface area, which improved the power storage capacity. After carbonization, carbon aerogels were obtained (Figure 1c). The surface of the carbon aerogel developed a network pore structure, and a large number of three-dimensional nanopores formed, which greatly improved the specific surface area. Figure 1d shows the carbon aerogel materials with 2.5 wt% GO. The surface of the material had a loose sponge-like structure, it means RGO was exactly implanted in the bamboo-derived cellulose fibers/RGO carbon aerogel composite as we expected and the graphene nanosheet layer was dispersed in the three-dimensional network pores of the carbon aerogel, which contributed to the conductivity of the composite material.

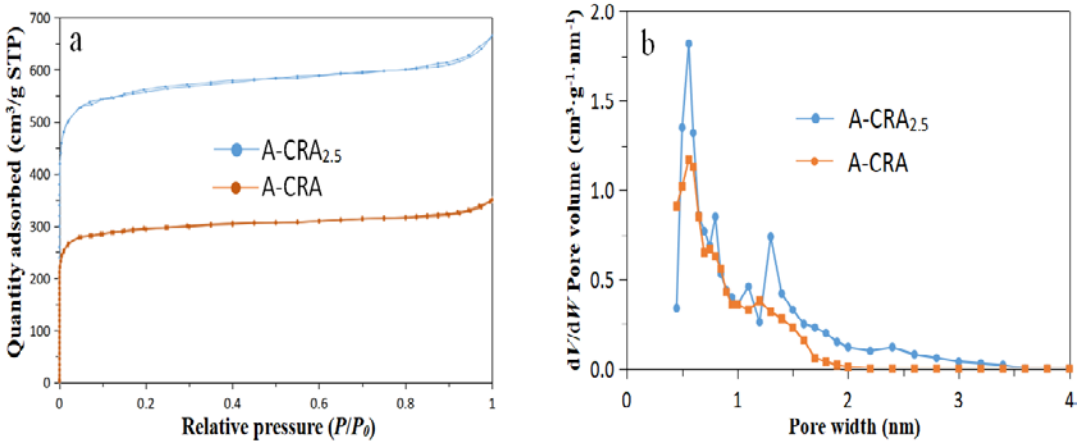

Figure 2. N_2 Adsorption Isotherms of A-CRA and A-CRA$_{2.5}$ (a) and Pore Size Distributions (b) of A-CRA and A-CRA$_{2.5}$

The SEM images of the carbon aerogel showed a large number of pore structures ranging from micro- to nanometer size. These macropores were mainly produced in the gel and regeneration process, which was controlled by the lyophilization and carbonization process. To characterize the micro- and mesopores in the material, we performed nitrogen adsorption/desorption tests on the sample A-CRA$_{2.5}$. Figure 2 shows the nitrogen adsorption/desorption isotherm and pore size distribution of A-CRA$_{2.5}$. The nitrogen adsorption of A-CRA increased sharply at relative pressures (P/P_0) less than 0.1, indicating the richer pore structure of the carbon aerogels after the KOH activation. Furthermore, the increase of the pressure curve saturation indicates that the material contained a large number of microporous structures, a hysteresis appeared in the range of $0.5 < P/P_0 < 1.0$, indicating that mesopores and macropores existed in A-CRA$_{2.5}$ [9]. The pore size distributions for the A-CRA and A-CRA$_{2.5}$ (Figure 2b) show that the A-CRA and A-CRA$_{2.5}$ have pores in the range of 0.5-2.0 nm and peaks appeared at 0.56, 0.8, and 1.3 nm, indicating A-CRA$_{2.5}$ with hierarchical pore structures. During

the KOH etching process, elemental potassium can embed into the carbon skeleton and creat voids with two times as large as the radius of potassium atoms (2.78 nm) is retained after elemental potassium is removed by HCl [10]. This result is consistent with the nitrogen adsorption/desorption isotherms. Moreover, the mesoporous and micropores increase the specific surface area of the composites from 1563 m^2/g for A-CRA to 1957 m^2/g for A-$CRA_{2.5}$. The loading of GO markedly increased the specific surface area and changed the pore distribution of carbon aerogels.

3.2. Chemical Characteristics of the Material

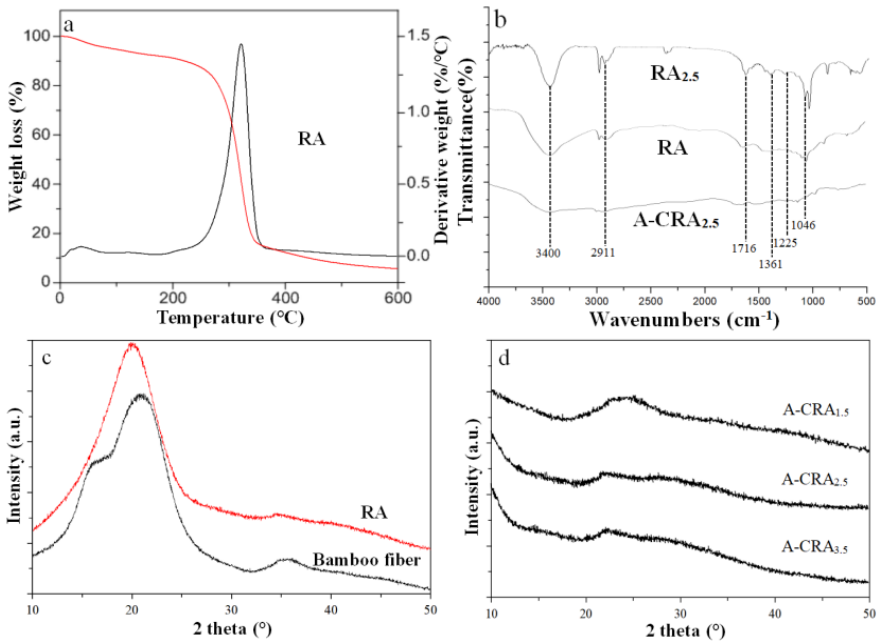

Figure 3. TG, DTG Curves for RA (a) and FTIR Spectra of RA, $RA_{2.5}$, A-$CRA_{2.5}$ (b) and X-ray Diffraction Patterns of Bamboo Fibers and RA (c), A-CRA_x (d)

We used thermogravimetric analysis (Figure 3a) to discover the carbonization temperature of bamboo cellulose fibers/GO aerogels. The mass loss of the bamboo cellulose aerogels over the range of 30-250 ℃ was only 5%, derived from moisture and carbon dioxide [11]. The aerogel pyrolysis temperature range was 250-350 ℃ and the mass loss rate was as high as 85%. The thermal decomposition rate of the largest peak temperature was 320 ℃, and the corresponding mass loss rate was 60%. This stage is mainly the result of cellulose glycosidic molecular chain decomposition, and a small amount of hemicellulose and lignin degradation/polycondensation reactions leading to pyrolysis and aromatic ring formation. Between 400–600 ℃ the mass loss is approximately 4%, which is attributable to a small amount of lignin degradation. These results further illustrate that the main constituent of the bamboo pulp fibers is cellulose. This is also consistent with the results in Table 1.

Figure 3b shows the FTIR spectra of RA, $RA_{2.5}$, and A-$CRA_{2.5}$. Characteristic peaks of cellulose appeared in the RA at 3400, 2911, 1466, 1361, and 1046 cm^{-1}, which are attributed to stretching vibration of O-H, CH_2, H-C-H and H-O-C bending vibration, and H-C-C, H-C-O, H-O-C bending vibration. In the spectrum of $RA_{2.5}$, characteristic peaks of GO appeared at 1716, 1361, and 1225 cm^{-1} respectively [12], corresponding to C=O stretching vibration of carboxyl group, C-H bending, and C-O stretching vibrations. By comparing the infrared spectra of RA and $RA_{2.5}$, we can see that the carbonyl absorption peak of the composite was increased significantly after adding GO. It can also further validate the XRD results that GO were implanted in the composite. After carbonization, the carbon aerogels showed no characteristic peaks of cellulose and only a small amount of inorganic H_2O and CO_2 absorption peaks. It shows that the basic structure of cellulose was destroyed and the oxygen-containing functional groups on GO were reduced.

Figure 3c shows XRD spectra of the bamboo pulp fibers and bamboo regenerated cellulose aerogel. Two characteristic peaks for cellulose appeared at 2θ = 16.3° and 22.0° in the bamboo pulp fibers, assignable to the (101) and (200) planes of type I cellulose respectively [13]. After regeneration, the bamboo regenerated cellulose aerogel was obtained. The peak at 16.3° disappeared and the peak width at 22.0° increased, indicating that the cellulose type I structure changed and converted to a cellulose type II structure. Figure 3d shows XRD results for the bamboo-derived cellulose fibers/RGO carbon aerogel composite with different contents of GO. All the patterns show a characteristic peak of graphene at approximately 11°, indicating that the GO was reduced during carbonization. Broad peak appeared at 22° shifted to higher angles as the increase of graphene content, indicating a higher degree of graphitization in the materials [14].

3.3. Electrochemical Performance

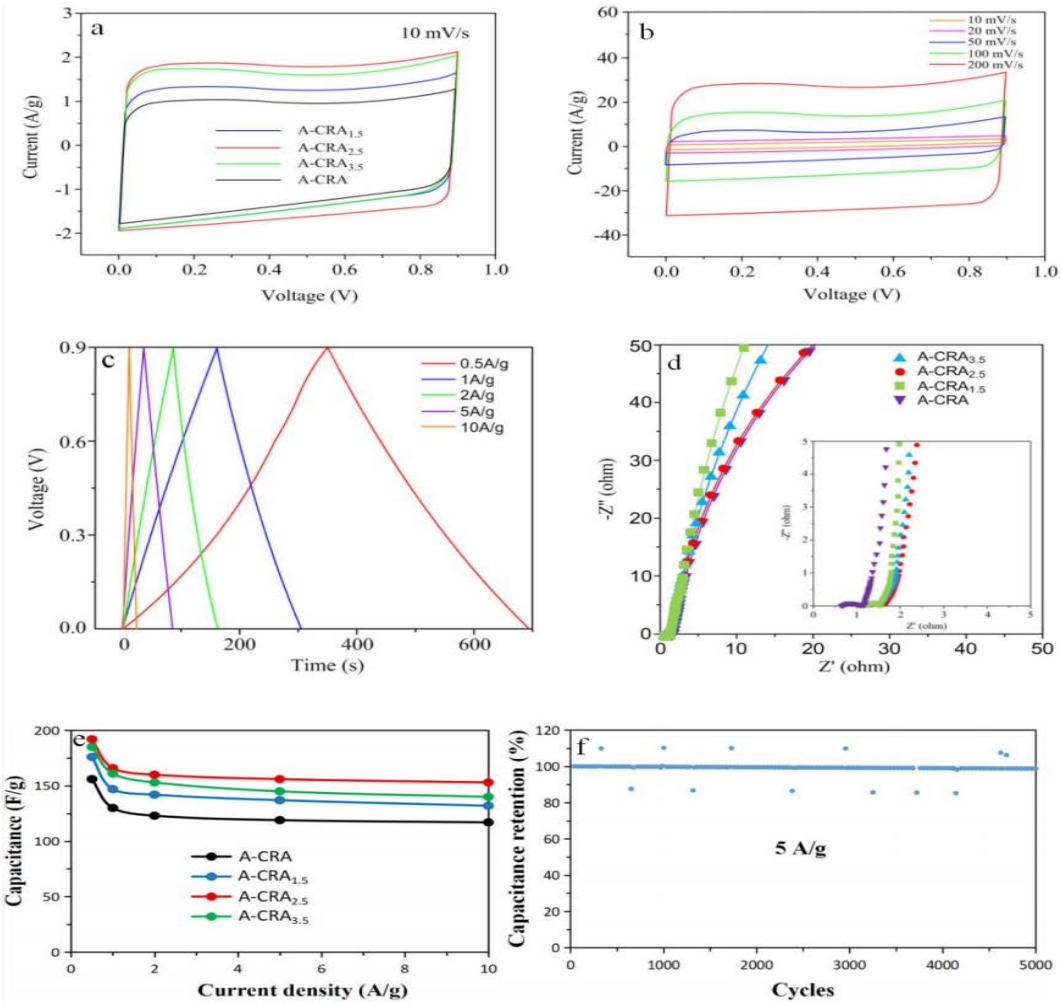

Figure 4. Electrochemical Properties of A-CRA$_x$ Samples in Three-Electrode Cell: CV Curves at Various Scan Rate of 10 mV/s (a); CV Curves of A-CRA$_{2.5}$ at Different Scan Rates (b); GCD Curves of A-CRA$_{2.5}$ Samples at Current Densities of 0.5-10 A/g (c); Nyquist Plots of A-CRA$_{2.5}$ (d); Capacitances at Different Current Densities (e); Cyclability for A-CRA$_{2.5}$ (f)

Figure 4a shows the CV curves of CRA and A-CRAx electrodes at a scanning rate of 10mV/s and a potential range of 0-0.9 V. The CV curve of CRA shows a deformed rectangle with a lower capacitance of 156 F/g. But the CV curve of A-CRAx showed a rectangular shape, indicating that a

perfect electrical double layer (reversible adsorption and desorption of ions) formed throughout the carbon network. The specific capacities of the A-$CRA_{1.5}$, A-$CRA_{2.5}$, and A-$CRA_{3.5}$ electrodes were 325, 351, and 334 F/g, respectively, at a scan rate of 10 mV/s and these values were 14%-24% higher than that of the A-CRA. The A-CRAx electrode maintained a good rectangular CV profile (Figure 4b) with the increase of scan rate. The A-$CRA_{2.5}$ sample had the maximum corresponding current and area under the CV curve (Figure 4a), indicating that it has the maximum specific capacitance, followed by that of the A-$CRA_{3.5}$ sample, and A-$CRA_{1.5}$ sample. Thus, the specific capacitance of carbon aerogels can be improved by the addition of GO. As the amount of GO was increased, the specific capacitance tended to increase. Figure 5b shows CV curves of A-$CRA_{2.5}$ at different scan rates which showed good performance of an electric double-layer capacitor. Even at a high scan rate of 200mV/s, the material maintained a symmetric rectangular shape suggesting that the material has good ratio performance [15].

As observed from the above results, the increase of graphene content in the composite resulted in an increase of the specific capacitance. However, as the GO content is increased up to a certain value, the specific capacitance of the composite material will decrease again. It probably because the graphene sheets would re-agglomerate, which reduces the overall specific surface area of the composite.

Figure 4c shows the GCD curves of A-$CRA_{2.5}$ under different current densities with all symmetrical triangles, indicating that the A-$CRA_{2.5}$ has high charge-discharge efficiency good electrolyte diffusion in the pore structures [16]. When the current density increased from 0.5 to 10 A/g, the specific capacitance of all the samples decreased, which was consistent with the CV data. When the current density was 0.5 A/g, the A-$CRA_{2.5}$ shows a capacitance of 192 F/g. When the current density increased to 10 A/g, the A-$CRA_{2.5}$ capacitance was maintained at 153 F/g. These results indicate that A-$CRA_{2.5}$ owns a good rate performance [17].

The resistance inside the electrode (Rs) reflects the power loss caused by itself. The smaller the internal resistance, the smaller the voltage drop caused by the internal resistance, indicating the small power loss, which is very important for the electrode material. In addition, supercapacitors also have a charge transfer resistance (Rct), which is a reflection of the resistance to charge movement. The smaller the charge transfer resistance, the better the electrical conductivity of the material. Figure 4d shows the EIS of A-CRAx. All samples show, almost perpendicular to the coordinate axis in the low-frequency region. The A-$CRA_{1.5}$ has the steepest curve, indicating a low diffusion resistance of electrolyte ions in its porous structure. In the high frequency region, the intercept between the curve and the coordinate axis is the resistance inside the electrode (Rs), which reflects a small charge transfer resistance (Rct) and the high current charge-discharge performance of the sample [18]. The Rct results for A-$CRA_{1.5}$, A-$CRA_{2.5}$, A-$CRA_{3.5}$, and A-CRA were 0.46, 0.30, 0.37, and 0.34 Ω. The test results show that the bamboo-derived cellulose fibers/RGO carbon aerogel composite has a small internal resistance and charge transfer resistance, indicating that the bamboo-derived cellulose fibers/RGO carbon aerogel composite has a small energy consumption and well electrical conductivity; it is completely suitable for supercapacitor electrode materials.

Figure 4eshows the capacitances of different samples at different current densities. It can be seen that when the current density increases from 0.5 A/g to 10 A/g, the specific capacitance of all samples presents a downward trend, and it declines rapidly in the range of low current density (0.5 A/g~1 A/g) and slowly in the range of high current density (2 A/g~10 A/g). At the same current density, the specific capacitance of A-$CRA_{2.5}$ is the largest, which is consistent with the detection result of CV. It is related to its large pore volume, wide pore distribution, smaller average pore and smaller internal resistance.

In order to characterize the cyclic stability of A-$CRA_{2.5}$, 5000 charge and discharge cycles were performed on the samples at the current of 5 A/g (Figure 4f). The specific capacitance retention rate is basically maintained above 99%, the results show that the material has good cyclic stability.

As we expected, we can see from the characterization of electrochemical properties that bamboo-derived cellulose fibers/RGO carbon aerogel composite have larger specific capacitance, well multiplier performance and rate performance, as well as excellent cyclic stability, these performances allow it to be used in the field of supercapacitor electrode materials.

4. Conclusions

In this experiment, we used tetrabutylammonium acetate/DMSO system to dissolve bamboo pulp fibers, the electrochemical properties of the materials were improved by doping RGO, and the porous structure of the materials were achieved by preparing the carbon aerogels. Finally, a porous bamboo-derived cellulose fibers/RGO carbon aerogel composite was obtained by freeze-drying and carbonization, which was then used as the electrode material for supercapacitors. The microstructures show a cross-linked fibers skeleton doped with porous nano-graphene sheets, with a specific surface area of 1957 m^2/g. Owing to these structural advantages, the material has a large specific capacitance (351 F/g). Lightweight, porous, and stable carbon aerogels show great promise as electrode materials for flexible ultracapacitors in the future. In addition, the preparation of green and environment-friendly regenerated cellulose carbon aerogel is a good way of applying biomass resources. Thus, these findings may also help to find new value-added applications for biomass materials.

5. Acknowledgments

This research was supported by the China Ministry of Science and Technology (2017YFD0600804).

6. References

[1] Dobashi A, Maruyama J, Shen Y, Nandi M, Uyama and Hiroshi 2018 Activated carbon monoliths derived from bacterial cellulose/polyacrylonitrile composite as new generation electrode materials in EDLC. *Carbohyd. Polym*. **200** 381-90

[2] Pérez-Madrigal M, Edo M, Saborío M, Estrany F and Alemán C 2018 Pastes and hydrogels from carboxymethyl cellulose sodium salt as supporting electrolyte of solid electrochemical supercapacitors. *Carbohyd. Polym.* **200** 456-67.

[3] Liu N, Shen J and Liu D 2013 Activated high specific surface area carbon aerogels for EDLCs. *Micropor. Mesopor. Mat*. **167** 176–81.

[4] Liang H, Guan Q, Chen L, Zhu Z, Zhang W and Yu S 2012 Macroscopic-Scale Template Synthesis of Robust Carbonaceous Nanofiber Hydrogels and Aerogels and Their Applications. *Angew. Chem. Int. Edit*. **51(21)** 5101–05.

[5] Ren F, Li Z, Tan W, Liu X, Sun Z, Ren P and Yan D 2018 Facile preparation of 3D regenerated cellulose/graphene oxide composite aerogel with high-efficiency adsorption towards Methylene blue. *J. Colloid. Interf. Sci*. **532** 58-67.

[6] Zu G, Shen J, Zou L, Wang F, Wang X, Zhang Y and Yao X 2016 Nanocellulose-derived highly porous carbon aerogels for supercapacitors. *Carbon.* **99** 203–11.

[7] Liu H, Wang A, Xu X, Wang M, Shang S, Liu S and Song J 2016 Porous aerogels prepared by crosslinking of cellulose with 1, 4-butanediol diglycidyl ether in NaOH/urea solution. *Rsc. Adv.* **6(49)** 42854-62.

[8] Sevilla M, Ferrero G and Fuertes A 2017 Beyond KOH activation for the synthesis of superactivated carbons from hydrochar. *Carbon*. **114** 50-8.

[9] Mi H, Jing X, Politowicz A, Chen E, Huang H and Turng L 2018 Highly compressible ultra-light anisotropic cellulose/graphene aerogel fabricated by bidirectional freeze drying for selective oil absorption. *Carbon*. **132** 199–209.

[10] Yang X, Fei B, Ma J, Liu X, Yang S, Tian G and Jiang Z 2018 Porous nanoplatelets wrapped carbon aerogels by pyrolysis of regenerated bamboo cellulose aerogels as supercapacitor electrodes. *Carbohyd. Polym.* **180** 385–92.

[11] Javadi A, Zheng Q, Payen F, Javadi A, Altin Y, Cai Z and Gong S 2013 Polyvinyl alcohol-cellulose nanofibrils-graphene oxide hybrid organic aerogels. *Acs. Appl. Mater. Inter*. **5(13)** 5969-75.

[12] Li C and Shi G 2014 Functional Gels Based on Chemically Modified Graphenes. *Adv. Mater*. **26(24)** 3992–4012.

[13] Hong K, Qie L, Zeng R, Yi Z, Zhang W, Wang D and Huang Y 2014 Biomass derived hard carbon used as a high performance anode material for sodium ion batteries. *J. Mater.Chem. A.* **2(32)** 12733.
[14] Hao P, Zhao Z, Tian J, Li H, Sang Y, Yu G, Cai H, Liu H, Wong C and Umar A 2014 Hierarchical porous carbon aerogel derived from bagasse for high performance supercapacitor electrode. *Nanoscale*. **6** 12120-9.
[15] Xu L, Guo M, Liu S and Bian S 2015 Graphene/cotton composite fabrics as flexible electrode materials for electrochemical capacitors. *Rsc. Adv.* **5(32)** 25244–9.
[16] Oschatz M, Boukhalfa S, Nickel W, Hofmann J, Fischer C, Yushin G and Kaskel S 2017 Carbide-derived carbon aerogels with tunable pore structure as versatile electrode material in high power supercapacitors. *Carbon*. **113** 283–91.
[17] Gao S, Li X, Li L and Wei X 2017 A versatile biomass derived carbon material for oxygen reduction reaction, supercapacitors and oil/water separation. *Nano. Energy.* **33** 334–42.
[18] Zhang Q, Wang Y, Zhang B, Zhao K, He P and Huang B 2018 3D superelastic graphene aerogel-nanosheet hybrid hierarchical nanostructures as high-performance supercapacitor electrodes. *Carbon*. **127** 449–58.